Universitat de les Illes Balears

MASTER'S THESIS

Thermal non-equilibrium in coronal loops

Adel Boul'harrak Abed

Master's Degree in Advanced Physics and Applied Mathematics

(Specialisation/Pathway *Astrophysics and Relativiy*)

Centre for Postgraduate Studies

Academic Year 2020-21

Thermal non-equilibrium in coronal loops

Adel Boul'harrak Abed

Master's Thesis

Centre for Postgraduate Studies

University of the Balearic Islands

Academic Year 2020-21

Key words:

Coronal loops, Thermal non-equilibrium, Magnetohydrodynamics

Thesis Supervisor's Name: Ramon Oliver

Contents

Chapter 1

Introduction

Astronomy has been a field of study for the human being since the ancient civilizations, with a especial interest on the star near the planet we inhabit, the Sun. One could think of the Sun as a rigid and quiet astronomical object, but since the first observation with a Telescope by Galileo until now, it has been proven by science that the Sun is always changing, full of activity.
Even though there is a big record of the solar activity, we still do not know everything about the Sun. Thanks to the development of technology, there are some powerful telescopes that can help improve the theoretical models. We have been able to observe, track and even measure some of the most important and beautiful phenomena of the solar atmosphere. If we talk about how the Sun is powered, over the past century, scientists have puzzled out the process of nuclear fusion as the Sun's power source for billions of years. Nonetheless, there is a key question that still has no answer: **How are the Solar Chromosphere and Corona heated?**

1.1 The million Kelvin mystery

1.1.1 Solar Structure

Before going any further in this work, we must understand the basic structure of the Solar atmosphere, which is commonly divided in 3 layers. The lowest is the photosphere, it is a shallow gas layer about 400 km deep and it is the optical 'surface' of the Sun. All the visible light is emitted from this layer, with a distribution in wavelength comparable to that of a black body. The photospheric temperature is about 5800 K. The second, intermediate, layer is the chromosphere, it is a layer of gas a few thousand kilometers thick and its light can only be seen during a total solar eclipse or using the appropriate filters. Usually the light from the chromosphere is too weak to be seen against the photosphere's brightness.

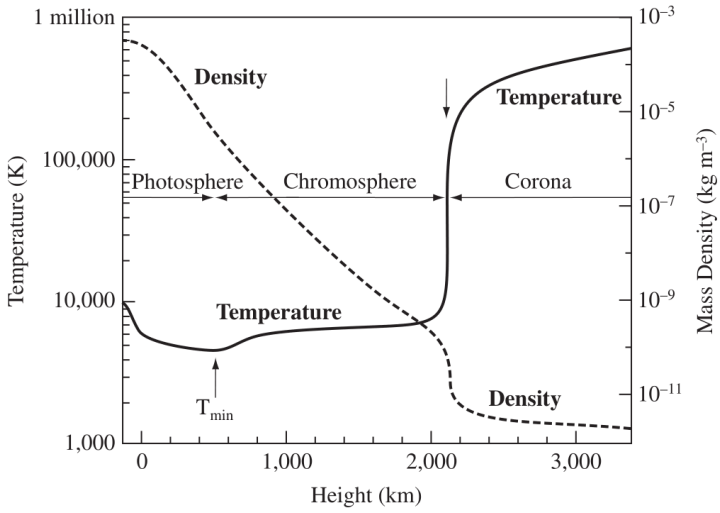

Figure 1.1: Mean variation of density (dashed line) and temperature (solid line) with height in the solar atmosphere. From Priest(2014) [1]

Now, here is the biggest mistery of the Sun. By the observations we know that the chromosphere is hotter than the photosphere. We are used to temperatures decreasing as distance from the heat source increases. Nevertheless, the temperature keeps increasing to the outermost part of the solar atmosphere reaching temperatures of a million Kelvin (see figure 1.1). This happens in the transition region, which is a very thin layer. Outside the transition region lies the hottest and largest part of the solar atmosphere, the solar corona. Brightness of the photosphere overpowers the light emitted from the Corona, therefore it can be only seen with the naked eyes during a solar eclipse and with an instrument that blocks the photospheric light from the image (coronagraph) or in UV wavelengths.

Some of the important solar activity stuctures can be observed on the chromosphere and the solar corona such as prominences, spicules, solar flares and coronal loops. In this work, we will focus our efforts on the study of coronal loops.

1.1.2 Coronal loops

The most basic definition a solar physicist will give you of a coronal loop is: coronal loops are conduits filled with heated plasma whose shape displays the geometry of the coronal magnetic field (Figure 1.2). In other words, coronal loops are magnetic field loops with both beginning and end on the Sun's surface which become visible due to the hot plasma that follows the coronal loops' magnetic field.

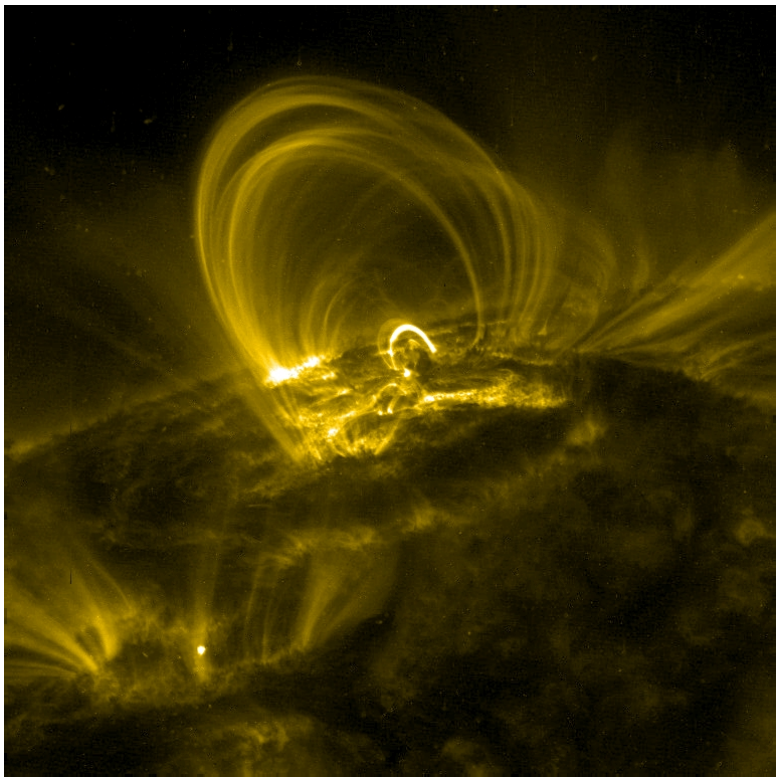

Figure 1.2: Example of coronal loop captured by NASA's Transition Region And Coronal Explorer (TRACE) with 171 $\AA$ filter.

But why do we want to study the coronal loops? My BS thesis presents a study of the coronal rain formation by catastrophic cooling and its dynamics. Coronal rain is this amazing phenomenon of cold blobs of plasma condensing at a loop and descending along one leg of the loop (Figure 1.3). The motivation of that work was the evidence shown in previous research that the coronal rain may give some knowledge of the spatial distribution of the heating in coronal loops or even give some hints to solve the big mystery, hence, be a marker for coronal heating mechanisms. For that reason, we need to understand this phenomenon as much as possible.

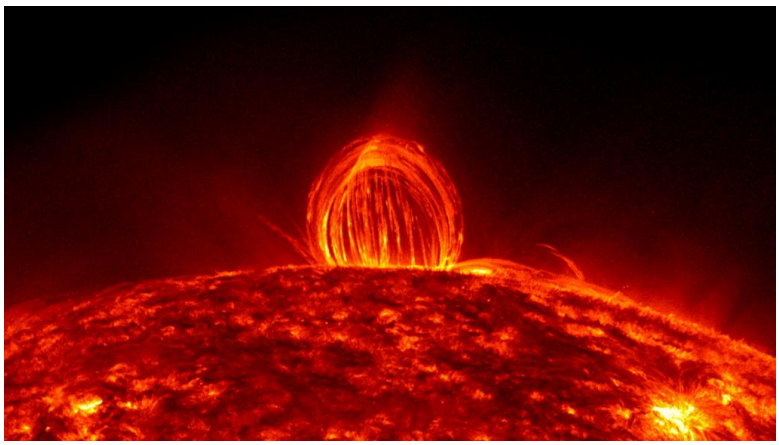

Figure 1.3: Example of coronal rain captured by NASA's Solar Dynamics Observatory (SDO) on 19th July 2012.

Coronal loops with heating concentrated at the footpoints, like the ones we considered in that work, can undergo a **thermal non-equilibrium** process (TNE), which can activate a process called catastrophic cooling that consists of dense blobs of plasma formed by the plasma cooling down to chromospheric temperatures.

Usually, on a same loop several plasma blobs can be observed in different time intervals, so thermal non-equilibrium process can also happen cyclic behaviour on the same coronal loop. Nonetheless while working on that analysis we realised that these coronal loops did not always lead to the TNE process. Thus, even the coronal rain being a far more common phenomenon than previously thought, we decided that before doing further research about coronal rain, the understanding of the TNE process on the coronal loops must be a priority.

1.2 Description of our reality: The magnetohydrodynamic equations

Before talking about TNE we need to do some math. Science is nothing without observation or theoretical description. In our case, we might say that the Sun is our plasma laboratory because any plasma theory can be checked directly by observation, mostly of the solar atmosphere.

The magnetohydrodynamic (MHD) equations are a great tool for the description of astrophysical plasma. Actually, the solar atmosphere plasma can be modeled impressively well by the ideal MHD equations. The basic assumptions made to get the ideal MHD approximation are:

- The plasma is a continuous medium and Maxwell's equations for the electric ($\vec{E}(\vec{r},t)$) and magnetic field ($\vec{B}(\vec{r},t)$) are considered.
- The rapid variations of electric and magnetic fields are not considered.
- No relativistic motions are considered. Therefore, the velocity of the particles is much smaller than c.
- Ohm's law is considered as the relation between the electric field and the current density vector ($\vec{j}(\vec{r},t)$).
- The electric conductivity is very high

MHD equations are nothing but a combination of the well known electromangetic equations (Maxwell's equations and Ohm's law) and fluid equations.

Maxwell's equations:

$$\nabla \wedge \vec{E} = -\frac{\partial \vec{B}}{\partial t}, \tag{1.1a}$$

$$\nabla \wedge \vec{B} = \mu\vec{j} + \frac{1}{c^2}\frac{\partial \vec{E}}{\partial t}, \tag{1.1b}$$

$$\nabla \cdot \vec{E} = \frac{\rho^*}{\epsilon}, \tag{1.1c}$$

$$\nabla \cdot \vec{B} = 0, \tag{1.1d}$$

Fluid equations[a]:

$$\frac{\partial \rho}{\partial t} + \nabla \cdot (\rho\vec{v}) = 0, \tag{1.2a}$$

$$\frac{Dp}{Dt} + \gamma p \nabla \cdot \vec{v} = -(\gamma - 1)\mathcal{L}, \tag{1.2b}$$

$$\rho\frac{D\vec{v}}{Dt} = -\nabla p + \frac{1}{\mu}(\nabla \wedge \vec{B}) \wedge \vec{B}. \tag{1.2c}$$

[a] Lagrangian operator, $\frac{D}{Dt} = \frac{\partial}{\partial t} + \vec{v} \cdot \nabla$.

Ohm's law [a]:

$$\vec{j} = \sigma\vec{E}, \tag{1.3}$$

[a] σ is the electrical conductivity.

where $\vec{E}$ is the electric field, $\vec{B}$ is the magnetic field, t is time, ρ is the plasma density, p is the plasma pressure,

$\vec{j}$ is the current density vector, $\rho^* = e(n^+ - n^-)$, with n^+ and n^- the number density of ions and electrons, μ is the magnetic permeability, ϵ is the permitivity of the plasma, c is the speed of light in vacuum, $c \approx 2.998$ x 10^8 m s^{-1}, $\gamma = 5/3$ is the ratio of specific heats and $\vec{v}$ is plasma velocity.

Second therm on the right-hand side of the equation (1.2c) is the Lorentz force. On the right-hand side of the energy equation (1.2b) we have the energy loss function, $\mathcal{L}$, which is given by a linear combination of radiative losses, heating and the effect of thermal conduction:

$$\mathcal{L} = R - H - \vec{\nabla} \cdot (\kappa \vec{\nabla} T), \tag{1.4}$$

where κ is the thermal conduction coefficient, H is the heating and the radiative losses (R) are defined as

$$R(T) = n_e n_p Q(T) \tag{1.5}$$

where n_e is the electron number density, n_p is the proton number density and $Q(T)$ is the radiative loss function (figure 1.4).

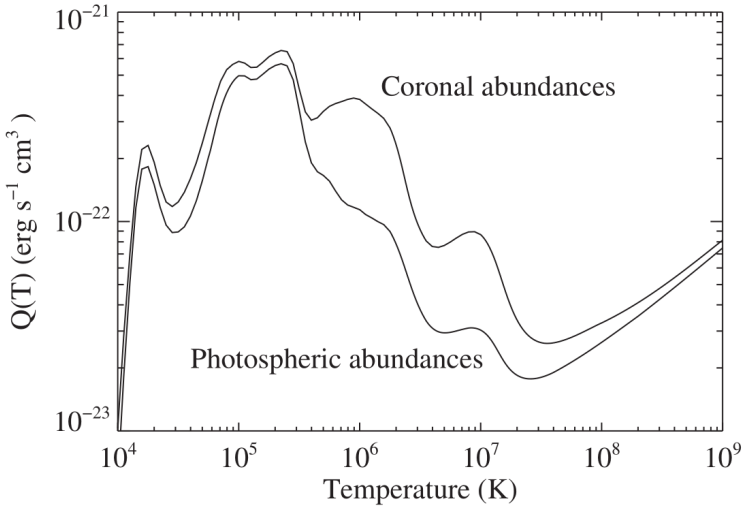

Figure 1.4: Radiative loss function $Q(T)$ for coronal (upper curve) and photospheric (lower curve) layers derived from observational data. (Source: Priest 2014 [1])

Therefore by combining the equations above we can write down the ideal MHD equations for non-adiabatic changes of state:

$$\frac{\partial \rho}{\partial t} + \nabla \cdot (\rho \vec{v}) = 0, \tag{1.6a}$$

$$\rho \frac{D\vec{v}}{Dt} = -\nabla p + \frac{1}{\mu}(\nabla \wedge \vec{B}) \wedge \vec{B}, \tag{1.6b}$$

$$\frac{Dp}{Dt} + \gamma p \nabla \cdot \vec{v} = -(\gamma - 1)\mathcal{L}, \tag{1.6c}$$

$$\frac{\partial \vec{B}}{\partial t} = \nabla \wedge (\vec{v} \wedge \vec{B}), \tag{1.6d}$$

$$\nabla \cdot \vec{B} = 0. \tag{1.6e}$$

Also, the equation of state is usually included,

$$p = \rho \frac{k_B}{m} T, \tag{1.7}$$

where k_B and m are the Boltzmann constant and the proton mass.

1.2.1 Linearized solutions to the hydrodynamics equations

One of the main lessons that we learn as physicists is to simplify as much as possible the problem that we are facing. Hence, in our case, a common approach to simulate the coronal loops is a 1D description. But, how or why can we do this? In coronal loops, in presence of the strong magnetic fields, heat conduction and plasma flows are aligned along the magnetic field lines, allowing a 1D description. Since the magnetic field is parallel to the loop axis, motions are only along the magnetic field and being the loop sufficiently thin, the only relevant variations are along its axis. Therefore, to get a solution for small perturbations, we will approach this problem by linearizing the equations of non-adiabatic hydrodynamics. For convenience, we will begin with the equations in the following form:

$$\frac{\partial \rho}{\partial t} + \nabla \cdot (\rho \vec{v}) = 0, \tag{1.8a}$$

$$\rho \left(\frac{\partial \vec{v}}{\partial t} + \vec{v} \cdot \nabla \vec{v} \right) = -\nabla p, \tag{1.8b}$$

$$\frac{1}{\gamma - 1} \frac{\partial p}{\partial t} + \frac{\nabla \cdot (\vec{v} p)}{\gamma - 1} = -p \nabla \cdot \vec{v} - \rho \mathcal{L} - \nabla \cdot \vec{q}, \tag{1.8c}$$

Where ρ, p, v are the density, pressure and velocity of the plasma. As mentioned above, the problem is simplified to a 1D hydrodynamic description. Thus, by using the following plane wave solutions where the background values are denoted with a "0" subscript, and the perturbation values with a "1" subscript,

$$\rho(x,t) = \rho_0(x) + \rho_1(x) e^{n\,t}, \tag{1.9a}$$

$$p(x,t) = p_0(x) + p_1(x) e^{n\,t}, \tag{1.9b}$$

$$v(x,t) = v_0(x) + v_1(x) e^{n\,t}, \tag{1.9c}$$

where, t is time, x is the spatial variable, n is the growth rate of the perturbation and the spatial part of the perturbation will be $e^{ik \cdot x}$, where k is the wave number, with a given amplitude, i.e $\rho_1 e^{ik \cdot x}$, since we are linearizing with a plane wave solution. A static and uniform background is assumed, therefore, p_0 and ρ_0 are constant values and $v_0 = 0$. Now, we introduce these solutions into the equations (1.8) to get the analytical solution. Because $\vec{q} = -\kappa(T) \nabla T$, and assuming that the Spitzer conductivity is $\kappa(T) = \chi(T) T^{5/2}$, we can write the perturbation of q as,

$$q_1 = -\kappa(T_0) \left(\frac{5}{2T_0} + \frac{1}{\chi} \frac{d\chi}{dT} \right) T_1 \nabla T_0 - \kappa(T_0) \nabla T_1 \tag{1.10}$$

We can neglect the first term because it does not enter into linear theory when perturbing a background flow with a uniform temperature. Also, as long as $T/|\nabla T|$ is much larger than the perturbation wavelength, we can take $\nabla T = 0$. So, for ∇q_1 we can approximate as

$$\nabla q_1 = -\kappa \nabla^2 T_1 \tag{1.11}$$

where T_1 can be eliminated by perturbating the ideal gas law,

$$\frac{T_1}{T_0} = \frac{p_1}{p_0} - \frac{\rho_1}{\rho_0}. \tag{1.12}$$

For the energy loss function perturbation we have

$$\mathcal{L}_1 = T_0 \mathcal{L}_{T,\rho} \left[\frac{p_1}{p_0} - \frac{\rho_1}{\rho_0} \right] + \rho_0 \mathcal{L}_{\rho,T} \frac{\rho_1}{\rho_0}, \tag{1.13}$$

where we use the notation $\mathcal{L}_{A,B} \equiv \left(\frac{\partial \mathcal{L}}{\partial A} \right)_B$. So, by replacing everything in equations (1.8) we get

$$n \rho_1 + ik \rho_0 v_1 = 0, \tag{1.14a}$$

$$n\rho_0 v_1 + ikp_1 = 0, \tag{1.14b}$$

$$\frac{1}{\gamma-1}np_1 + \frac{1}{\gamma-1}ikp_0v_1 = -\rho_1\mathcal{L}_0 - \rho_0T_0\mathcal{L}_{\mathcal{T},\rho}\left[\frac{p_1}{p_0} - \frac{\rho_1}{\rho_0}\right] + \rho_0^2\mathcal{L}_{\rho,\mathcal{T}}\frac{\rho_1}{\rho_0} - k^2\kappa T_0\left[\frac{p_1}{p_0} - \frac{\rho_1}{\rho_0}\right]. \tag{1.14c}$$

From equations (1.14a) and (1.14b) if we take A as a free parameter as $A \equiv \rho_1/\rho_0$, we can write the other perturbation amplitudes as function of ρ_1 as

$$v_1 = A(in/k), \tag{1.15a}$$

$$p_1 = -A\rho_0(n/k)^2, \tag{1.15b}$$

and we take into consideration that $n = n_R + in_I$, where n_R is the real part of n and n_I the imaginary part we have

$$\rho(x,t) = \rho_0 + A\rho_0 e^{n_R t}\cos(n_I t + kx), \tag{1.16a}$$

$$p(x,t) = p_0 + A\rho_0 e^{n_R t}\left[\frac{2n_R n_I}{k^2}\sin(n_I t + kx) - \frac{n_R^2}{n_I^2}k^2\cos(n_I t + kx)\right], \tag{1.16b}$$

$$v(x,t) = -Ae^{n_R t}\left[\frac{n_I}{k}\cos(n_I t + kx) + \frac{n_R}{k}\sin(n_I t + kx)\right]. \tag{1.16c}$$

We are interested on the condensation or thermal mode solution, which is the one with $n_I = 0$. On the other hand, for $n_R = 0$ we have the acoustic wave solution, where all variables vary in phase, and if $n_R \neq 0$ the acoustic wave can be damped or over-stable as function of the n_R sign. Thus, with n_R, we can get the analytic solution describing the thermal mode which corresponds to the condensation process in the linear regime of thermal instability:

$$\rho(x,t) = \rho_0 + A\rho_0 e^{n_R\, t}\cos(k\, x), \tag{1.17a}$$

$$p(x,t) = p_0 - A\left(\frac{n_R}{k}\right)^2 e^{n_R\, t}\cos(k\, x), \tag{1.17b}$$

$$v(x,t) = -A\left(\frac{n_R}{k}\right) e^{n\, t}\sin(k\, x). \tag{1.17c}$$

In this work we will consider a system with fixed boundaries, thus we are interested on standing waves. So, to get a standing wave we have superposition of waves traveling from opposite directions,

$$\rho(x,t) = \rho_0 + 2A\rho_0 e^{n_R\, t}\cos(k\, x), \tag{1.18a}$$

$$p(x,t) = p_0 - 2A\left(\frac{n_R}{k}\right)^2 e^{n_R\, t}\cos(k\, x), \tag{1.18b}$$

$$v(x,t) = -2A\left(\frac{n_R}{k}\right) e^{n_R\, t}\sin(k\, x), \tag{1.18c}$$

where n_R is the growth rate of the perturbation of the thermal mode.

1.3 Thermal non-equilibrium and Thermal Instability

Thermal instability (TI) may play an important role in the formation of coronal rain plasma condensations during a TNE cycle. Klimchuk [2] argues that thermal instability and thermal non-equilibrium are fundamentally different by the initial state of the loop. Thermal instability is understood as a perturbation introduced into a steady state. With TNE, the loop is constantly looking for an inexistent equilibrium. Klimchuk points out that during a TNE cycle the formation of a condensation cannot be a thermal instability given that a coronal loop undergoing TNE is out of equilibrium.

There are reasons that suggest that plasma condensations, such as coronal rain, would not come only from TNE, which is a global phenomenon, but must be caused by thermal instability because these condensations require a localized effect. There are many works following that reasoning (Antolin [3], Claes and Keppens [4]).

One of the main objectives of this work is to predict the stability of a coronal loop and demonstrating that thermal conduction plays an important role. The first approach to thermal instability was carried out by Field [5], but for a static and homogeneous medium. Balbus [6] revisited Field's work and conducted research towards a dynamic medium, which fits more the structure studied in our work. Nevertheless, thermal conduction was still excluded in the formulation of an instability criterion. The type of condensations analysed in this work, coronal rain, grow in the isobaric regime. For this reason, we consider the isobaric instability criterion defined by (Waters and Proga [7]), where they get to the Balbus' criterion for TI including the effect of thermal conduction:

$$\left[\frac{\partial(\mathcal{L}/T_0)}{\partial T}\right]_p < -\frac{\Lambda_0}{T_0^2}\left(\frac{\lambda_F}{\lambda}\right)^2, \tag{1.19}$$

where λ is the perturbation wavelength, $\mathcal{L}$ is the energy loss function, T_0 is the background temperature, Λ_0 is the net cooling rate and λ_F is the Field length, which is defined as

$$\lambda_F \equiv 2\pi\sqrt{\left(\frac{\kappa T}{\rho\Lambda}\right)}\Bigg|_0. \tag{1.20}$$

In figure 1.6 we can see in which range of values of temperature and mass density the coronal plasma is thermally unstable.

Currently it is not yet clear wether TI plays any role in the formation of coronal rain plasma condensations during a TNE cycle. Thus, in order to shed some light on this discussion, we revisit the Balbus [6] instability criterion to determine if in our coronal loop simulations there are perturbations with a growth rate fast enough (compared with the TNE cycle time scales) to form condensations.

Research mentioned above, where thermal instability in coronal loops is explored, does not include an important component, thermal conduction. Even being a stabilizing factor, at high temperatures thermal conduction becomes very important in the thermodynamics of coronal loops. As we can see in Figure 1.5, where growth rate from Field [5] for the thermal mode is computed by solving the dispersion relation, the growth rate reaches negative values above $1.5 \cdot 10^6$ K when thermal conduction is included (solid line).

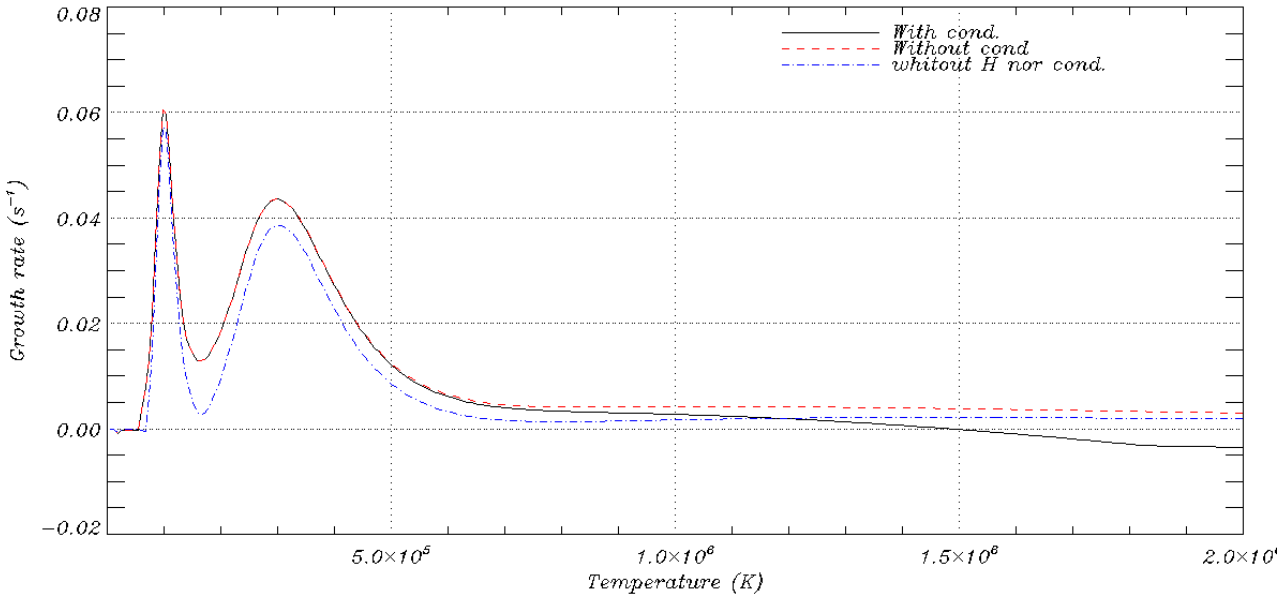

Figure 1.5: Comparison of the condensation mode growth rate obtained by solving the dispersion relation from Field [5] with a fixed mass density of $\rho_0 = 1.5 \cdot 10^{-11}$. The solid line is the case solved including the thermal conduction, the red dashed line is the case solved without thermal conduction and the blue dashed line is the case solved without heating and without thermal conduction.

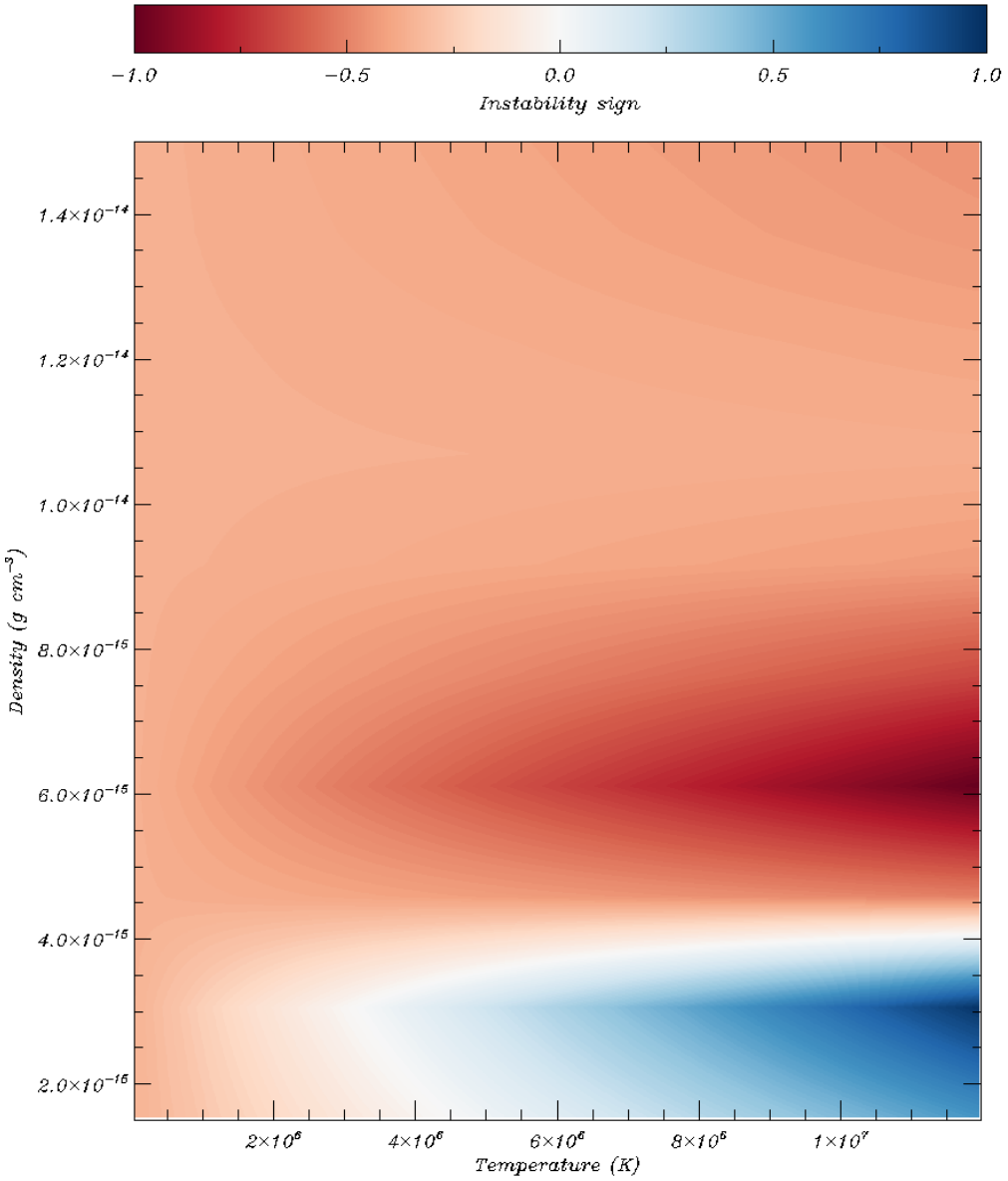

Figure 1.6: 2D plot of the isobaric instability criterion: $\left[\frac{\partial(\mathcal{L}/T_0)}{\partial T}\right]_p + \frac{\Lambda_0}{T_0^2}\left(\frac{\lambda_F}{\lambda}\right)^2 < 0$. Red indicates negative values, thus instability and blue indicates positive values, thus stability.

By making a cut into figure 1.6 through a given typical coronal mass density value (see Figure 1.7), we can see that once coronal temperatures are reached the criterion predicts thermal stability. This result links up with Figure 1.5 where the importance of thermal conduction has been shown.

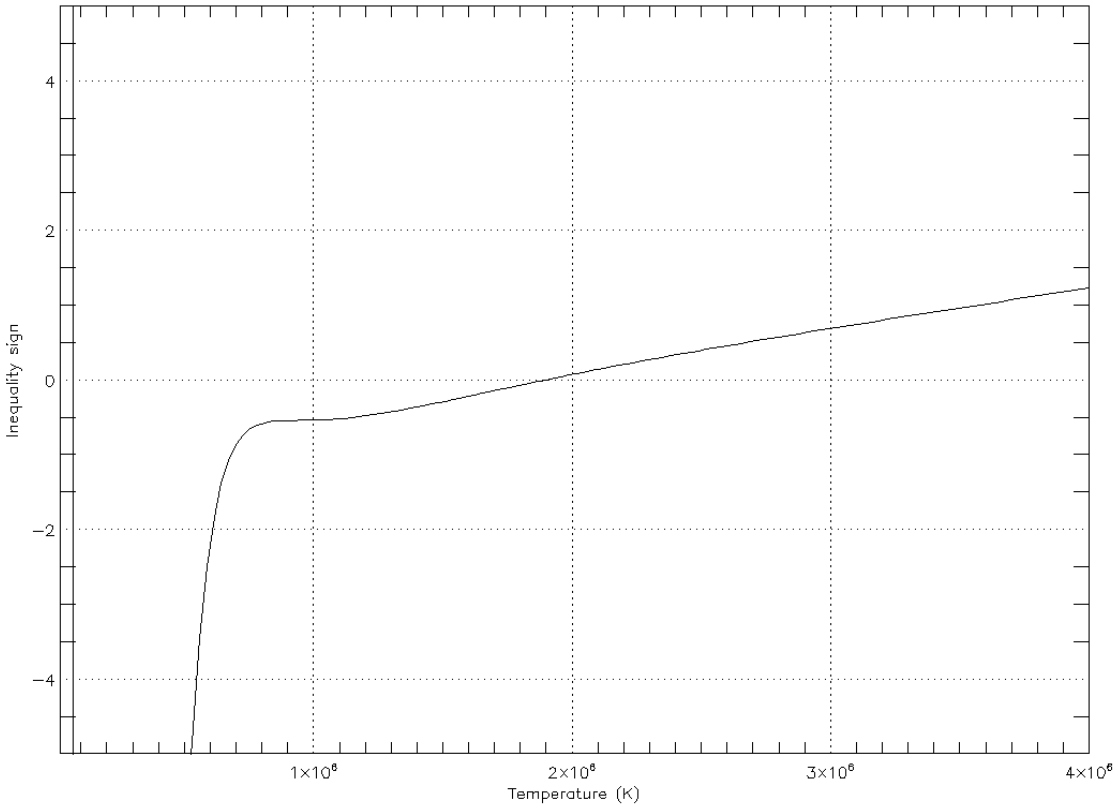

Figure 1.7: Instability sign represented as function of temperature with a fixed mass density $\rho = 1.5 \cdot 10^{-15}$ g cm^{-3}. Negative values indicate instability and positive values indicate stability.

Now, by solving the dispersion relation from Field 1965 [5] for a uniform medium we can also get a 2D representation of the stability of the medium as function of the plasma instability growth rate. In figure 1.8 we can see a similar representation of the stability of a plasma as function of density and temperature, for coronal values, where for each ρ and T all the growth rates values are computed for a wide range of wave numbers, by solving the dispersion relation obtained from the linearization of the hydrodynamics equations. Thus, if all the growth rate numbers are negative, the plasma will be stable, hence represented with the blue color, and otherwise, plasma will be unstable, hence represented with red color. We can see that for a given temperature we can have the same situation as density changes, but at $\approx 2 \times 10^5$ K and $\approx 1 \times 10^4$ K, where we can find a transition from unstable to stable as density increases. But if we take a fixed density plasma, we can see that there is a change on the stability as temperature changes.

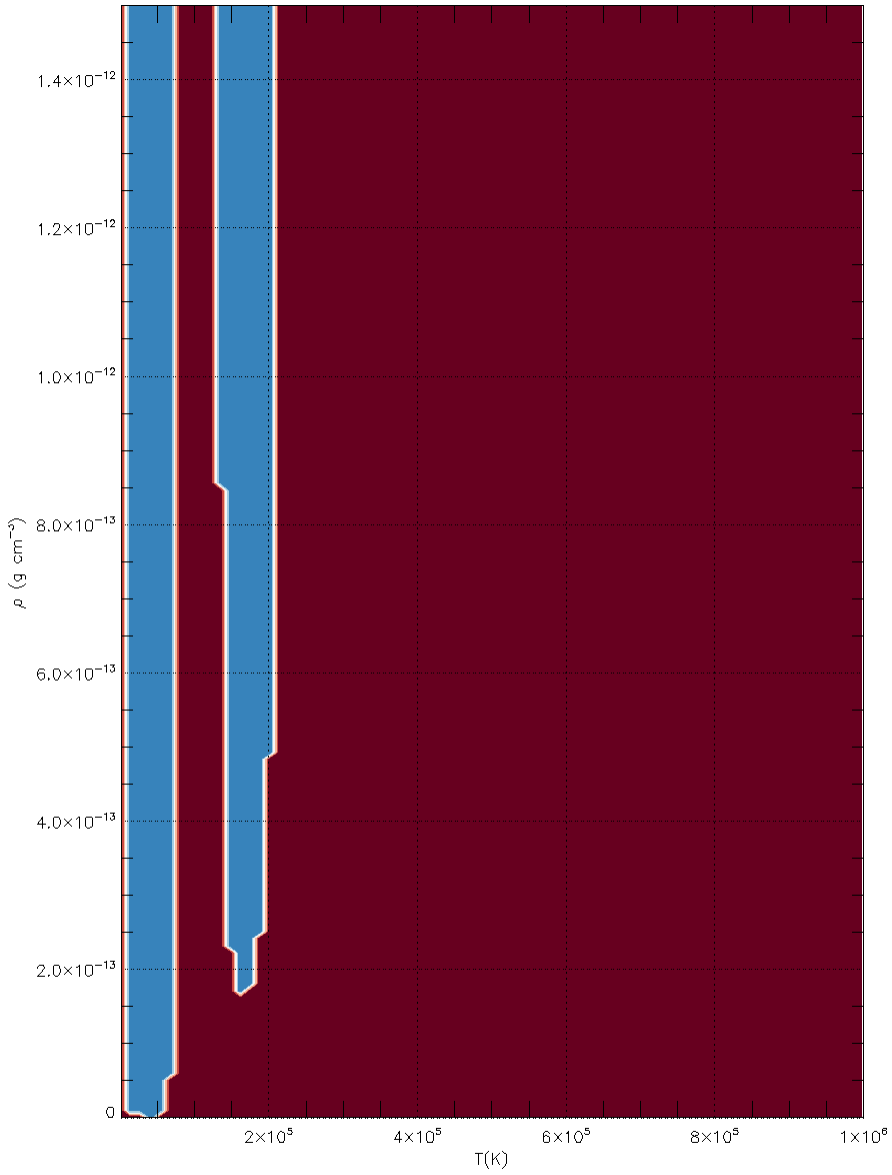

Figure 1.8: 2D plot of plasma stability where y axis is density and x axis is temperature, red color represent instability and blue color represents stability.

On this work we will focus on the behaviour of the plasma with different parameter settings. We will be exploring not only the change of temperature and density, but also different wavelengths when using sinusoidal perturbations (eq. 1.10) and other perturbation functions.

Chapter 2

Numerical Results

2.1 Numerical model

Equations 1.8 are solved using the numerical code named molMHD (insertar referencia a algun articulo de jaume donde se mencione el codigo), which solves the non-linear ideal MHD equations in 3D based on the method of lines (mol). For the time dependence 4th order Runge-Kutta is used. Uniform mesh of points is used, with one ghost cell in each boundary, extrapolation is made for all the variables except for the velocity components which are set to zero. The variables presented in this section are dimensionless, so spatial variable x is x/L, where L is the system length, and time is t/t_0, where $t_0 = L/C_s$, where C_s is the adiabatic sound speed.

2.2 Analytical Solutions

First, we want to check that the numerical model can reproduce the expected analytic solutions for the linear regime (eq. 1.8). So, we set the simulation initial perturbation (equations 1.18 with $t = 0$ with the following parameters:

- Temperature $= 1 \cdot 10^6$ K.
- Density $= 1.5 \cdot 10^{-12}$ kg m^{-3}.
- $A = 1 \cdot 10^{-3}$
- $n_R = 0.00015$ s^{-1}

As we can see in figure 2.1, the perturbation follows the analytical solution along the linear regime. Since the analytical solutions have an exponential time dependence, it is almost a must to do a linear fit of the time evolution for a fixed spatial point in a logarithmic scale. From figure 2.2 we can get the same information, displayed in another way. The solid line remains over the red dashed line, which represents the linear fit, until the linear regime is over, where the perturbation no longer has an exponential behaviour.

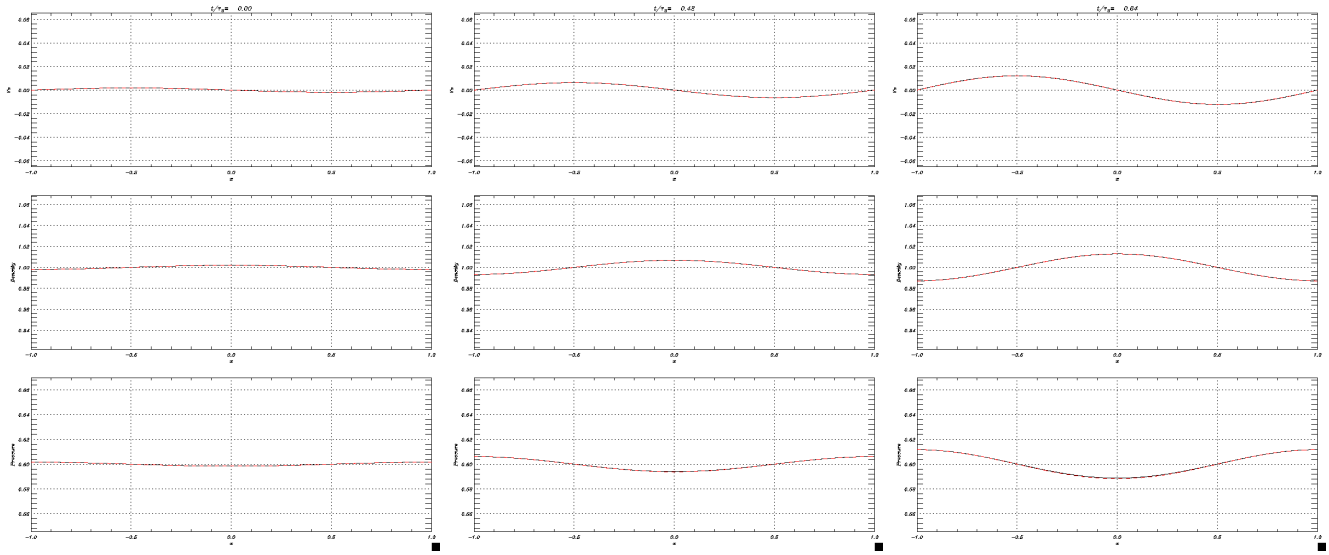

(a) t = 0 (b) t = 0.42 (c) t = 0.64

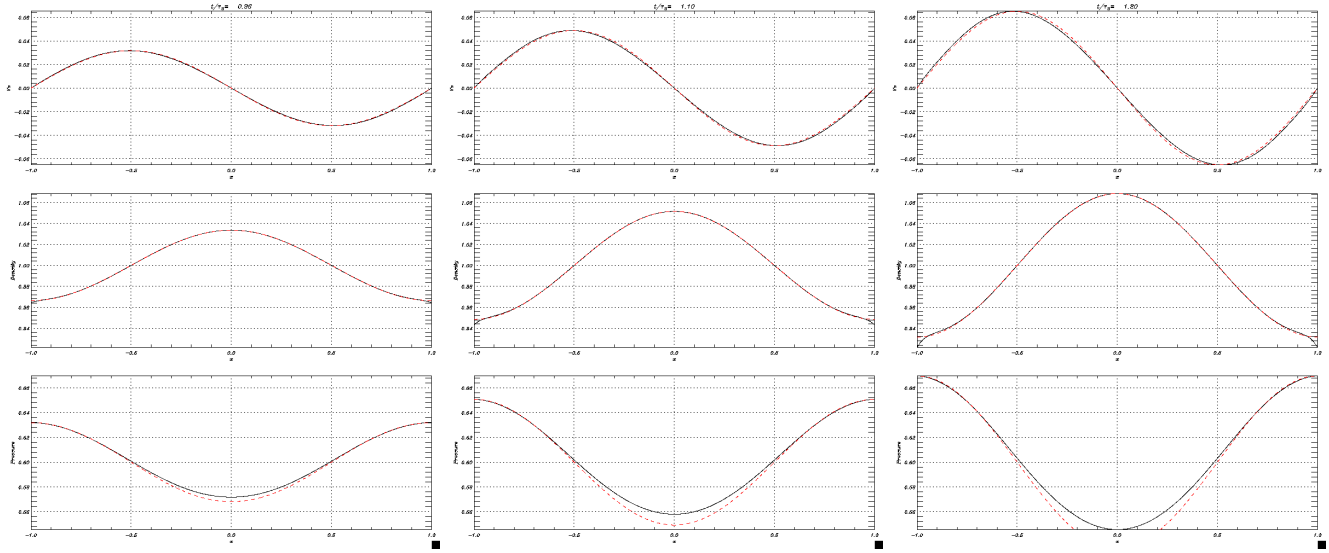

(d) t = 0.96 (e) t = 1.10 (f) t = 1.20

Figure 2.1: Time evolution of a sinusoidal perturbation with $1 \cdot 10^6$ K plasma temperature, $\rho_0 = 1.5 \cdot 10^{-12}$ kg m^{-3} plasma density, $A = 1 \cdot 10^{-3}$ perturbation amplitude, $n_R = 1.5 \cdot 10^{-3}$ s^{-1} perturbation growth rate and $L = \pi/1 \cdot 10^{-9}$ m system length. First panel is velocity in the x direction, second panel is density and third panel is pressure, all as function of space. The solid line represents the numerical result and the red dashed line is the analytical solution. In the x-axis we have x/L, so the spatial variable is dimensionless.

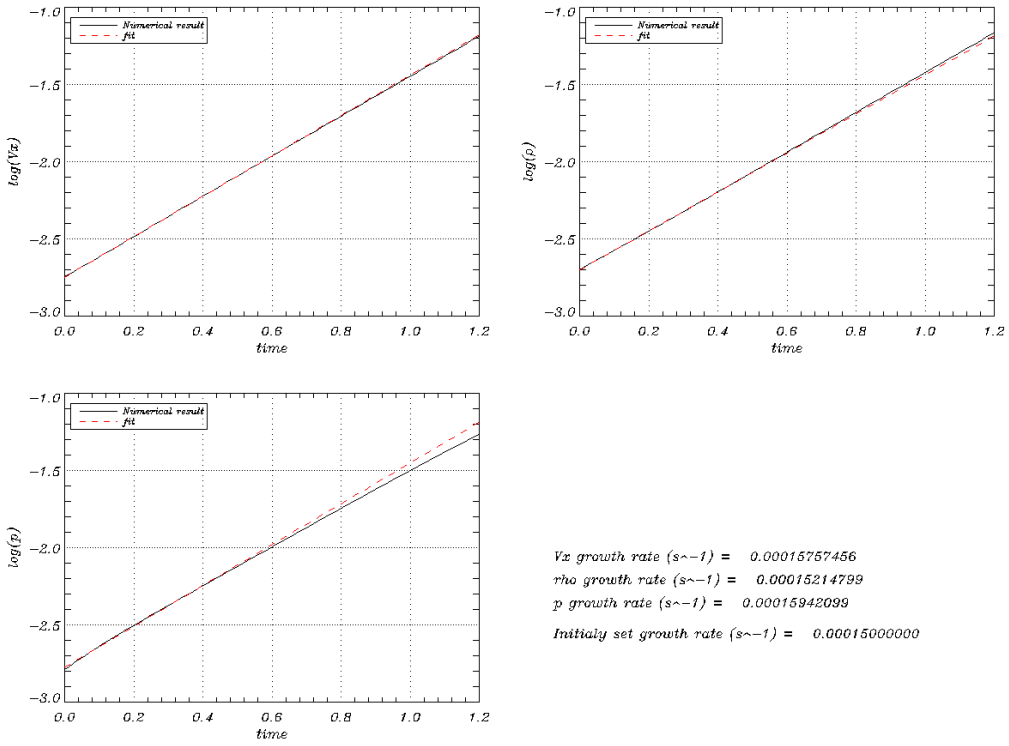

Figure 2.2: Time evolution of a fixed point for every variable in logarithmic scale of the simulation from Figure 2.1. Solid line represents the time evolution of the variable and the red dashed line is the linear fit.

In this case, the perturbation follows the expected linear regime behaviour until $t \approx 0.6$, which can be clearly seen on the linear fit (figure 2.2). Now we run different simulations where we permute some parameters to see how a perturbation evolves under certain situations.

2.2.1 Changing temperature with fixed density and wave number

If we check again figure 1.8, we can see that for a fixed density we will find different situations for a perturbation as temperature changes. Here we are going to show two simulations with different temperatures. We take the simulation presented on the previous section and then another one with $T = 10^4$ K. So, the simulation with $T = 10^4$ K is set as follows:

- Temperature $= 1 \cdot 10^4$ K.
- Density $= 1.5 \cdot 10^{-12}$ kg m^{-3}.
- $A = 1 \cdot 10^{-3}$
- $n_R = -2.46 \cdot 10^{-5}$ s^{-1}

Given that the growth rate is negative, the perturbation will damp in time over time (see figure 2.3). This is not the reason for the discrepancy between the analytical and numerical solutions. The point is that although you select an initial disturbance that corresponds to the condensation mode, you are not setting this initial disturbance with infinite precision. You must have also deposited a tiny amount of energy on some slow modes (or even other condensation modes with a slower rate of decrease). When the amplitude of the condensation mode has gone below the amplitude of these slow modes, the later start being visible. The numerical solution diverges from the analytical solution around $t \approx 0.30$. Even though we select an initial perturbation corresponding to the condensation mode, the initial disturbance is not set with infinite precision. So, there is a small amount of energy on some slow modes. Then, when the amplitude of the condensation mode has gone below the amplitude of these slow modes, the later start being visible. Now, we take a fixed spatial point and check the time evolution on a logarithmic scale, since the temporal part of the analytical solution is

an exponential. Thus we have figure 2.4, where we can see a solid line that represents the numerical solution and a red dashed line which represents a linear fit to the numerical solution.

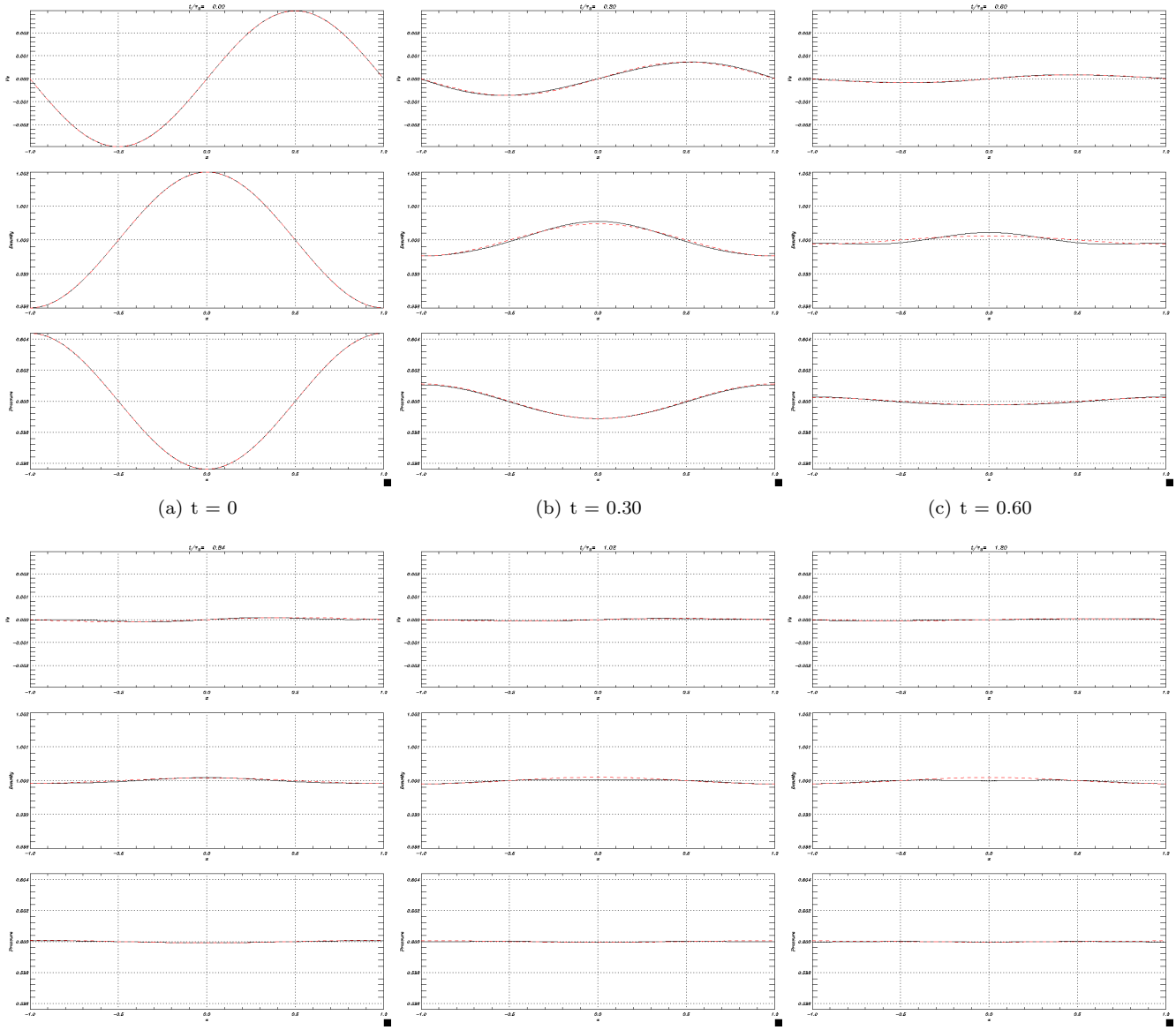

(a) t = 0 (b) t = 0.30 (c) t = 0.60

(d) t = 0.84 (e) t = 1.02 (f) t = 1.20

Figure 2.3: Time evolution of a sinusoidal perturbation with $1 \cdot 10^4$ K plasma temperature, $\rho = 1.5 \cdot 10^{-11}$ kg m^{-3} plasma density, $A = 1 \cdot 10^{-3}$ perturbation amplitude, $n = 1.5 \cdot 10^{-3}$ s^{-1} perturbation growth rate and $L = \pi/1 \cdot 10^{-9}$ m system length. First panel is velocity in the x direction, second panel is density and third panel is pressure, all as function of space. The solid line represents the numerical result and the red dashed line is the analytical solution.

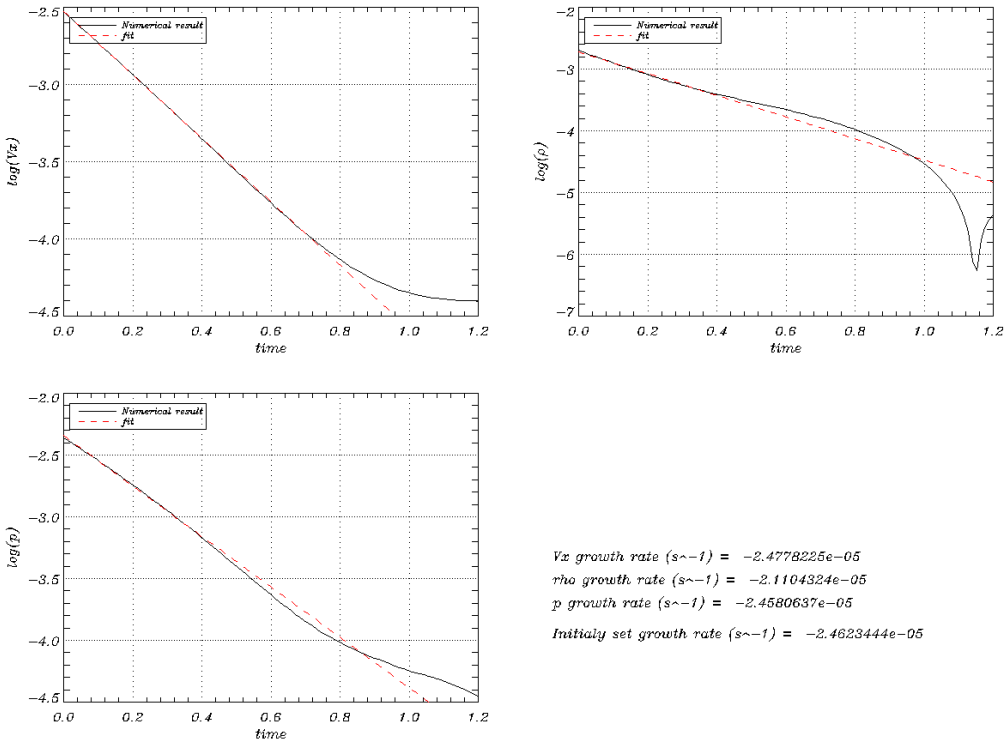

Figure 2.4: Time evolution of a fixed point for every variable in logarithmic scale of the simulation from Figure 2.3. Solid line represents the time evolution of the variable and the red dashed line is the linear fit.

We wonder which would be the effect of changing the amplitude of the perturbation, A. We take the two previous simulations and decrease the amplitude of the perturbation. Simulation 2.1, decreasing the amplitude to $A = 10^{-5}$. As we can expect, the linear regime gets prolonged in time, as we can see in figure 2.5. A more neat point of view can be obtained if a comparison of the linear fits is made. So, for the case with $A = 10^{-5}$ (figure 2.6) the linear fit and the logarithmic time evolution overlap longer than the simulation where $A = 10^{-3}$. Nonetheless, non-linear evolution appear in the system boundaries which are not observable in the linear fit (figure 2.5). Thus, we can see that the linear regime breaks at $t \approx 1.55$, which is one unit of time over the case with a higher perturbation amplitude.

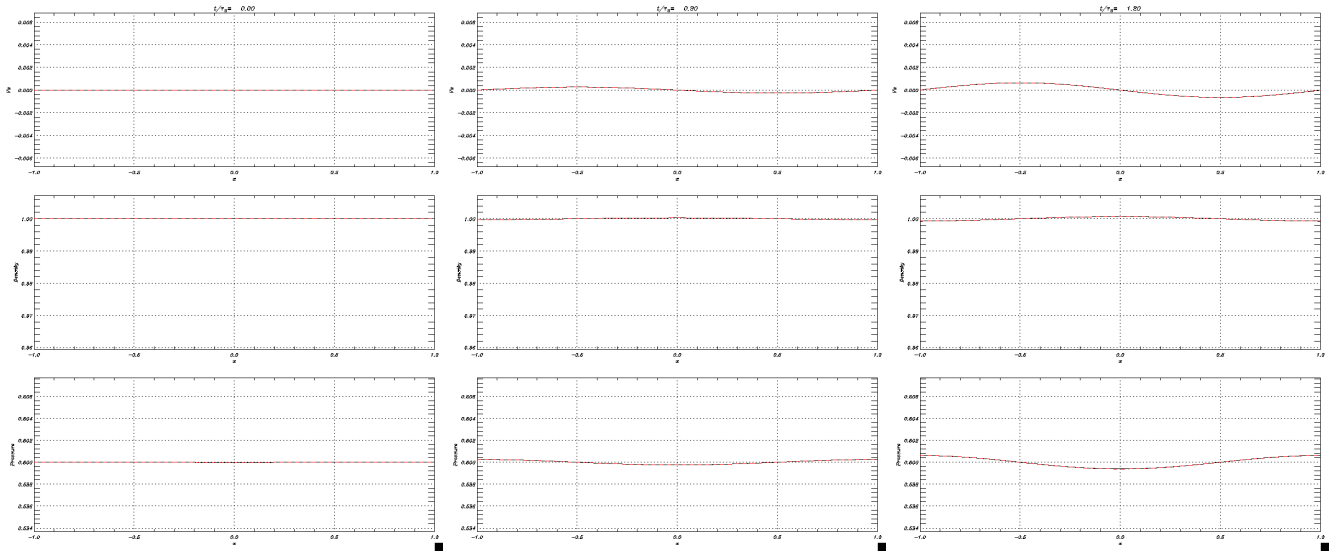

(a) t = 0 (b) t = 0.90 (c) t = 1.20

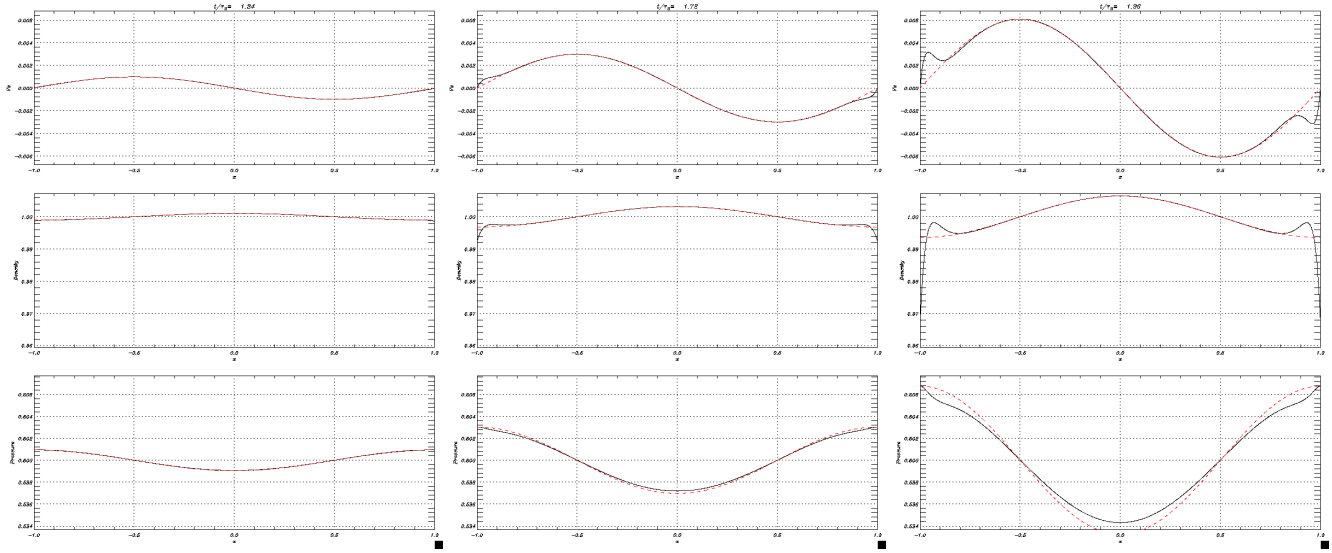

(d) t = 1.34 (e) t = 1.72 (f) t = 1.96

Figure 2.5: Time evolution of a sinusoidal perturbation with $1 \cdot 10^4$ K plasma temperature, $\rho = 1.5 \cdot 10^{-12}$ kg m^{-3} plasma density, $A = 1 \cdot 10^{-5}$ perturbation amplitude, $n = 1.5 \cdot 10^{-3}$ s^{-1} perturbation growth rate and $L = \pi/1 \cdot 10^{-9}$ m system length. First panel is velocity in the x direction, second panel is density and third panel is pressure, all as function of space. The solid line represents the numerical result and the red dashed line is the analytical solution.

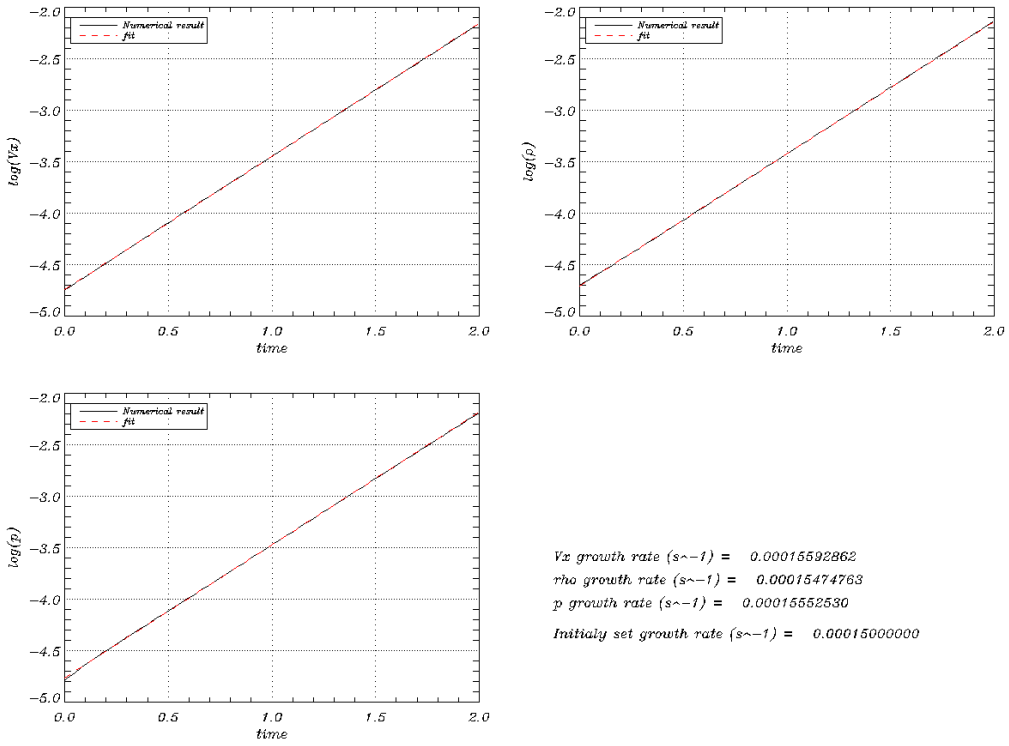

Figure 2.6: Time evolution of a fixed point for every variable in logarithmic scale of the simulation from Figure 2.5. Solid line represents the time evolution of the variable and the red dashed line is the linear fit.

For the case of the negative growth rate, figure 2.7, a similar result is obtained, the linear regime is longer in simulation where the perturbation amplitude is lower, and non-linear regime is reached after a longer period of time in the simulation (Figure 2.6). Therefore, the lower the amplitude of the perturbation, the longer the plasma remains in the linear regime, since less energy will be deposited into acoustic modes and the amplitude of the condensation mode is bigger for a longer period of time.

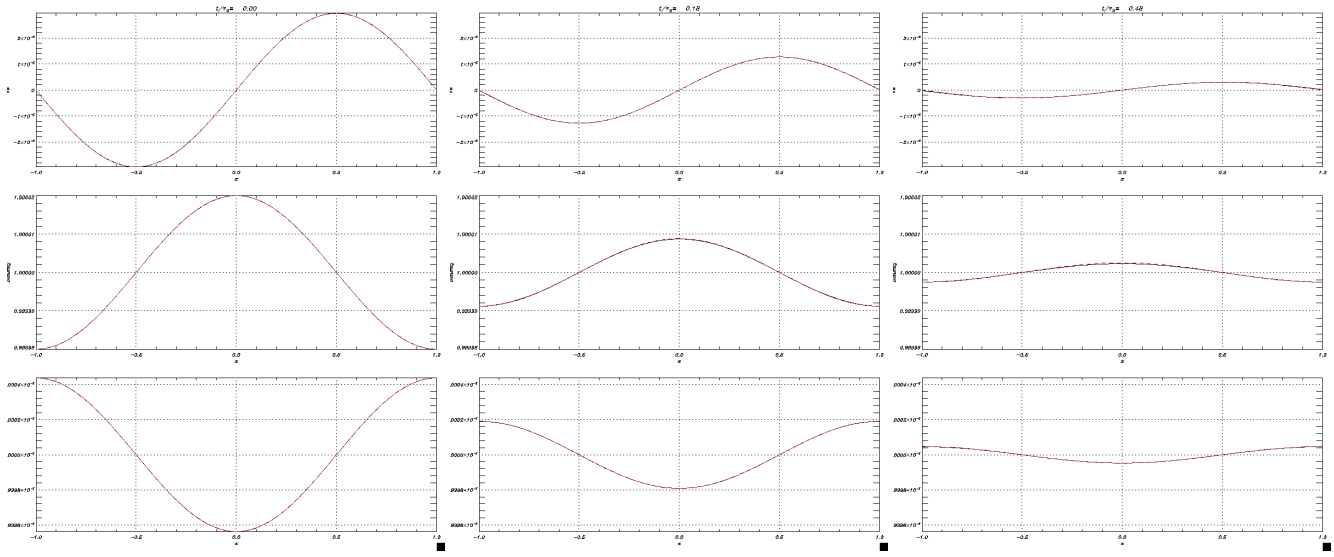

(a) t = 0 (b) t = 0.18 (c) t = 0.48

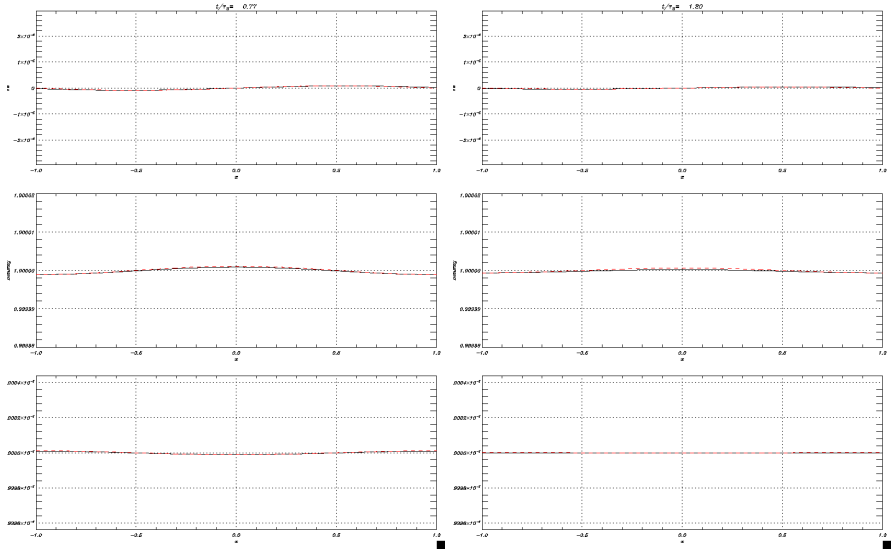

(d) t = 0.77 (e) t = 1.20

Figure 2.7: Time evolution of a sinusoidal perturbation with $1 \cdot 10^4$ K plasma temperature, $\rho = 1.5 \cdot 10^{-11}$ kg m^{-3} plasma density, $A = 1 \cdot 10^{-3}$ perturbation amplitude, $n = 1.5 \cdot 10^{-3}$ s^{-1} perturbation growth rate and $L = \pi/1 \cdot 10^{-9}$ m system length. First panel is velocity in the x direction, second panel is density and third panel is pressure, all as function of space. The solid line represents the numerical result and the red dashed line is the analytical solution.

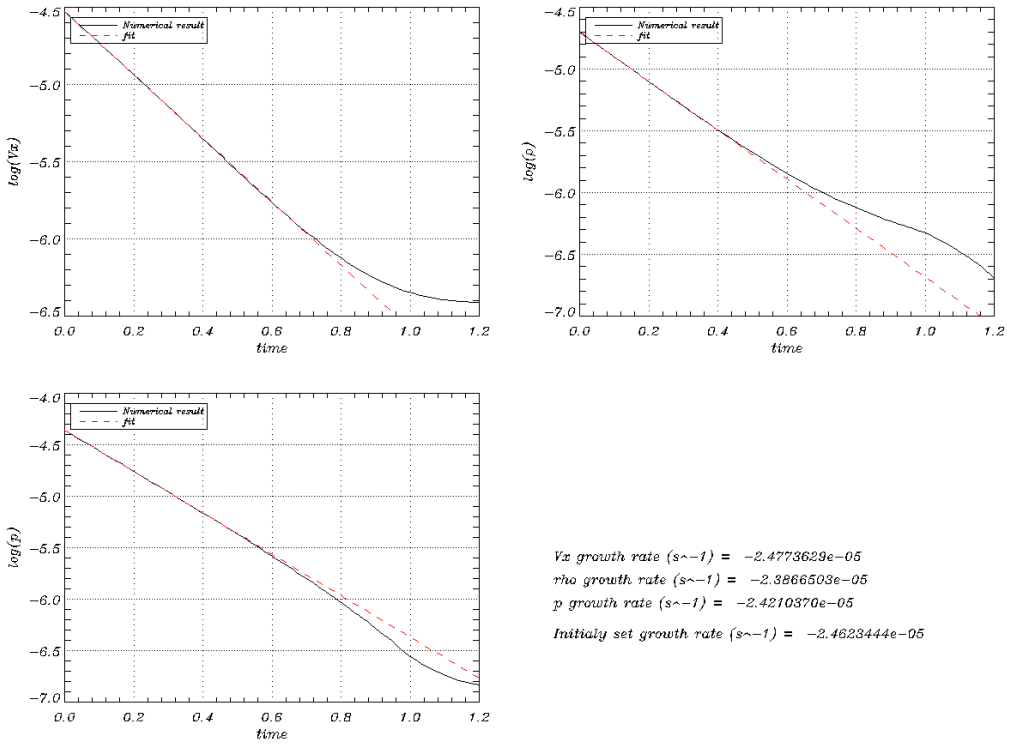

Figure 2.8: Time evolution of a fixed point for every variable in logarithmic scale of the simulation from Figure 2.7. Solid line represents the time evolution of the variable and the red dashed line is the linear fit.

2.2.2 Changing number of nodes with fixed temperature and density

Following the same steps that have been taken in this work, another parameter that can be changed is the wave number, which modifies the number of nodes of the analytical solution. Thus, we will repeat the simulation with a positive growth rate and see how different wave lengths, λ, impacts the perturbation time evolution.

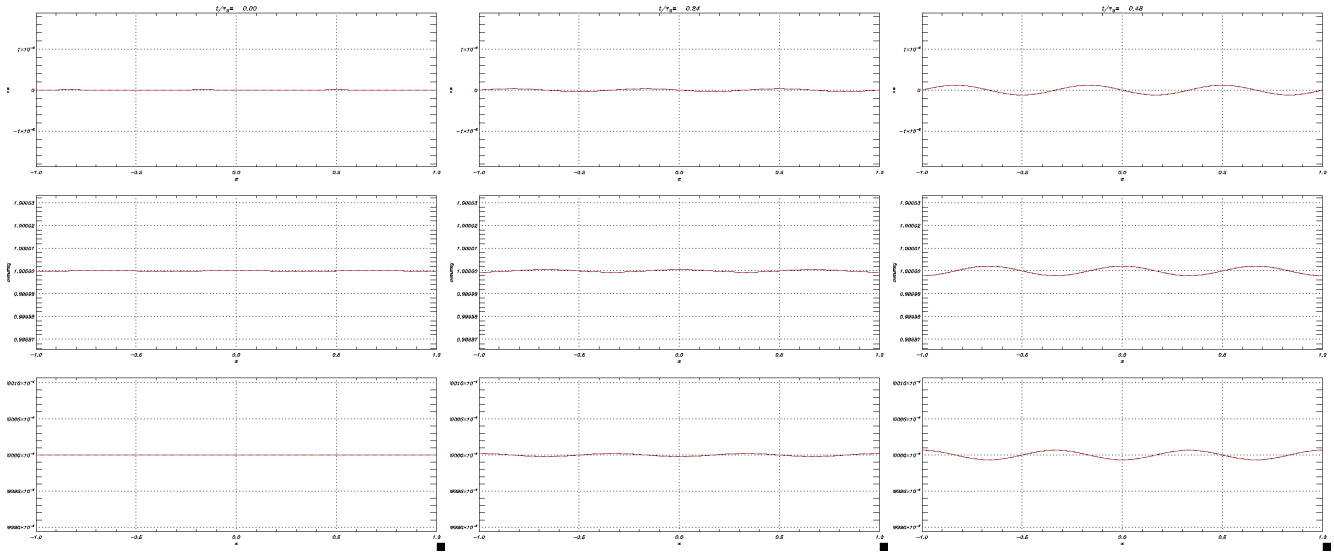

(a) t = 0 (b) t = 0.24 (c) t = 0.48

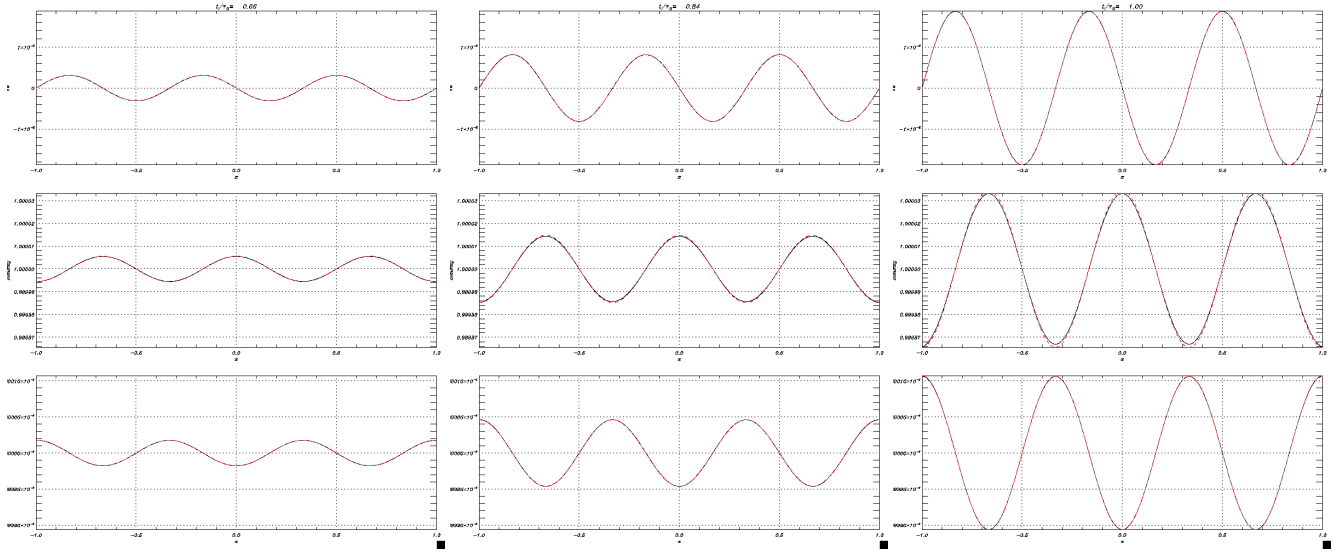

(d) t = 0.68 (e) t = 0.84 (f) t = 1.00

Figure 2.9: Time evolution of a sinusoidal perturbation with $1 \cdot 10^4$ K plasma temperature, $\rho = 1.5 \cdot 10^{-12}$ kg m^{-3} plasma density, $A = 1 \cdot 10^{-5}$ perturbation amplitude, $n = 1.5 \cdot 10^{-3}$ s^{-1} perturbation growth rate and $L = \pi/1 \cdot 10^{-9}$ m system length. First panel is velocity in the x direction, second panel is density and third panel is pressure, all as function of space. The solid line represents the numerical result and the red dashed line is the analytical solution.

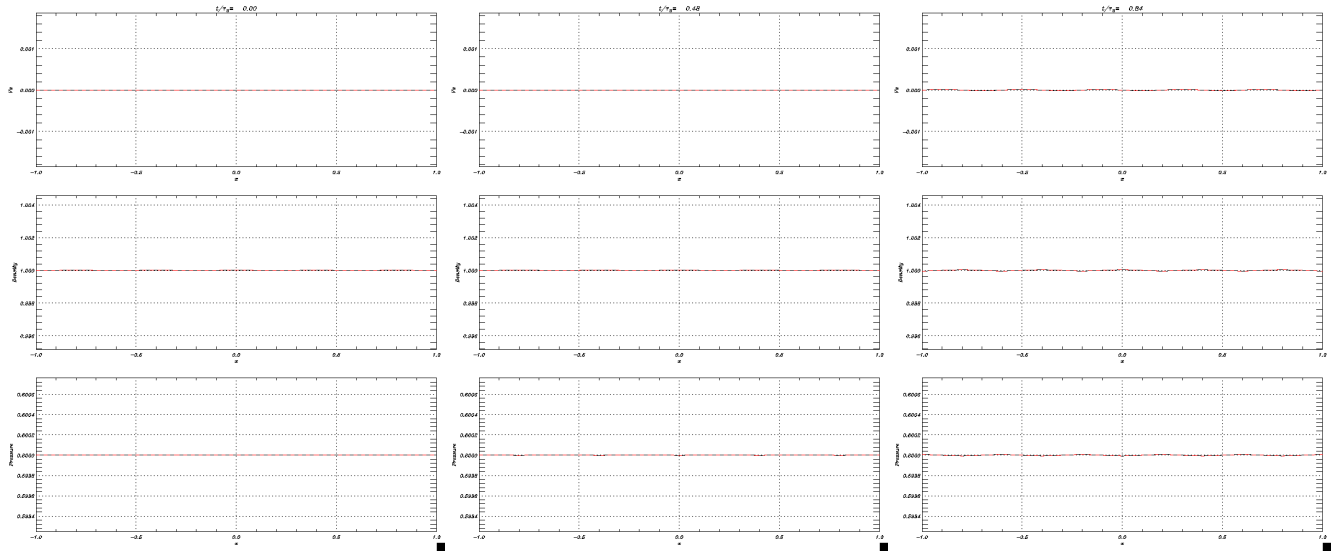

(a) t = 0 (b) t = 0.48 (c) t = 0.84

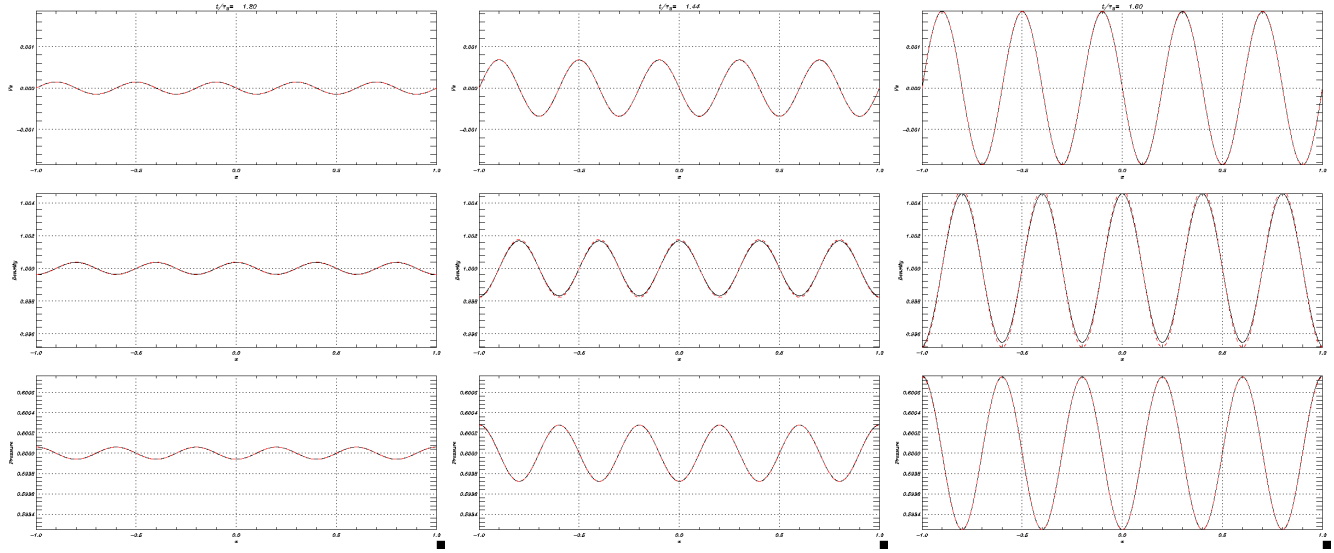

(d) t = 1.20 (e) t = 1.44 (f) t = 1.60

Figure 2.10: Time evolution of a sinusoidal perturbation with $1 \cdot 10^4$ K plasma temperature, $\rho = 1.5 \cdot 10^{-12}$ kg m^{-3} plasma density, $A = 1 \cdot 10^{-5}$ perturbation amplitude, $n = 1.5 \cdot 10^{-3}$ s^{-1} perturbation growth rate and $L = \pi/1 \cdot 10^{-9}$ m system length. First panel is velocity in the x direction, second panel is density and third panel is pressure, all as function of space. The solid line represents the numerical result and the red dashed line is the analytical solution.

For the case with a positive growth rate, we can see how the perturbation grows longer into the linear regime as higher number of nodes are in the solution. When the perturbation is a sinusoidal wave with 3 nodes, figure 2.9, the linear regime has a longer time period. So one can only wonder what would be the effect if more nodes are added to the perturbation function. Therefore, we have simulation shown in figure 2.10 which has a 5 node sinusoidal perturbation, where the perturbation remains even a longer period of time in the linear regime. Thus, as more nodes are added to the perturbation, it appears to have a more consistent linear behaviour.

2.3 Gaussian perturbation

On most simulations where perturbations on solar atmosphere, mostly on solar corona, are placed the Gaussian function is most commonly used because a Gaussian distribution is a simple representation of a localised disturbance. Thus, in this work we will also carry out some simulations where the initial perturbations on density are expressed as Gaussians as function of space. On first simulation, our Gaussian is set as follows:

- Centered on $x = 0$ with $\sigma^2 = 0.002$
- Amplitude $A = 10^{-4}$

where the perturbation on density has the form of

$$\rho(x,t) = \rho_0 + \frac{A}{\sigma\sqrt{2\pi}} e^{\frac{-x^2}{2\sigma^2}} \tag{2.1}$$

Both situations with negative and positive growth rate, n_R.

Simulation from figure 2.11 which has the same parameters as simulation from figure 2.1, shows a perturbation with a dominant growth behaviour. Since not only thermal mode is excited, but also the acoustic modes, a superposition of modes are expected to be present until the dominant takes over the plasma evolution. In the case for the first simulation (figure 2.11), the thermal mode is clearly imposing over the other modes, so the perturbation grows until it reaches a numerical singularity in the simulation.

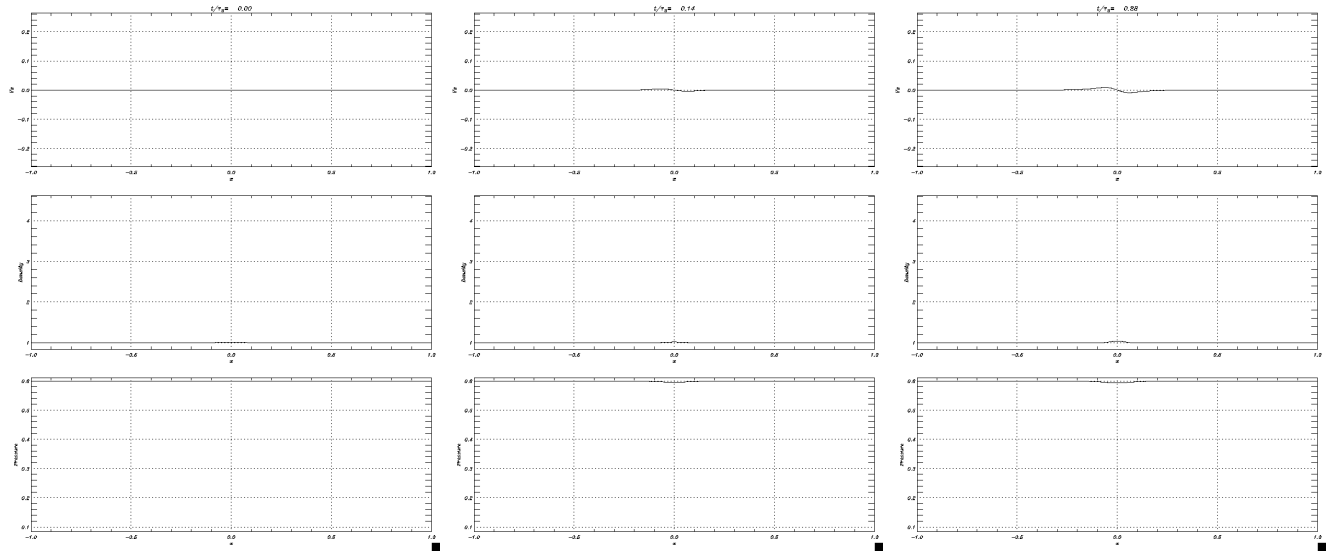

(a) t = 0 (b) t = 0.14 (c) t = 0.28

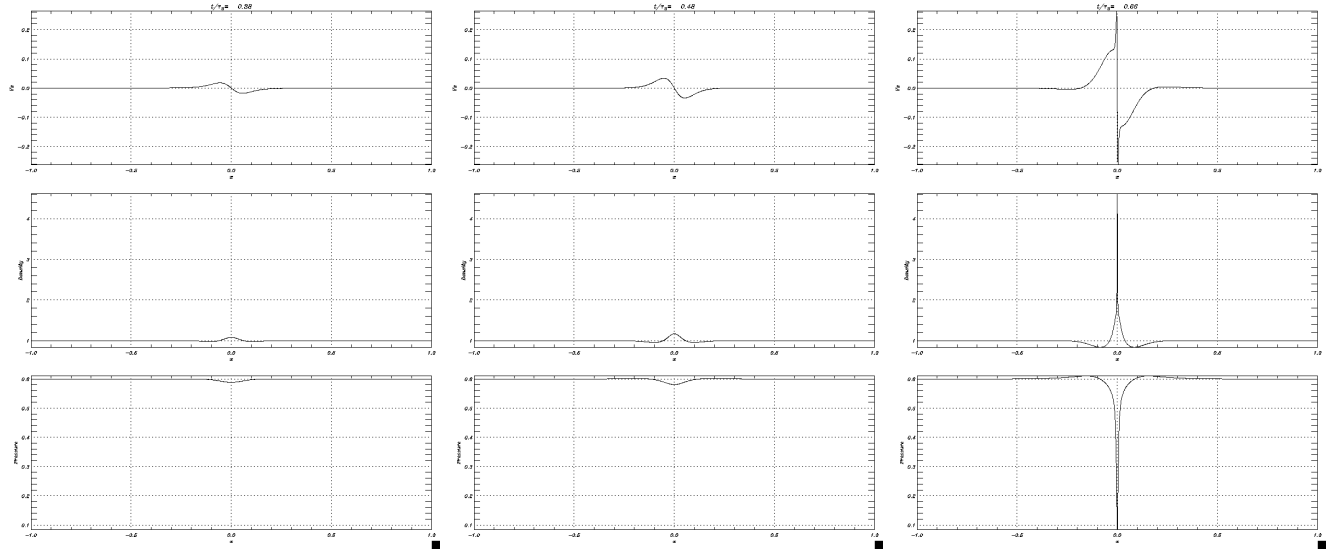

(d) t = 0.38 (e) t = 0.48 (f) t = 0.66

Figure 2.11: Time evolution of a gaussian perturbation with $1 \cdot 10^6$ K plasma temperature, $\rho = 1.5 \cdot 10^{-12}$ kg m^{-3} plasma density, $A = 1 \cdot 10^{-3}$ perturbation amplitude and $L = \pi/1 \cdot 10^{-9}$ m system length. First panel is velocity in the x direction, second panel is density and third panel is pressure, all as function of space. The solid line represents the numerical result.

Nonetheless, as we can see in figure 2.12 in the case where we set the same temperature and density values of simulation from figure 2.3, even although a thermal mode is expected to overcome the rest, acoustic modes appear to have a big role in the perturbation time evolution. Therefore, we can see how the perturbation dissipates through time, with a gradient of pressure pushing the plasma towards both ends of the system, until the perturbation gets dissipated.

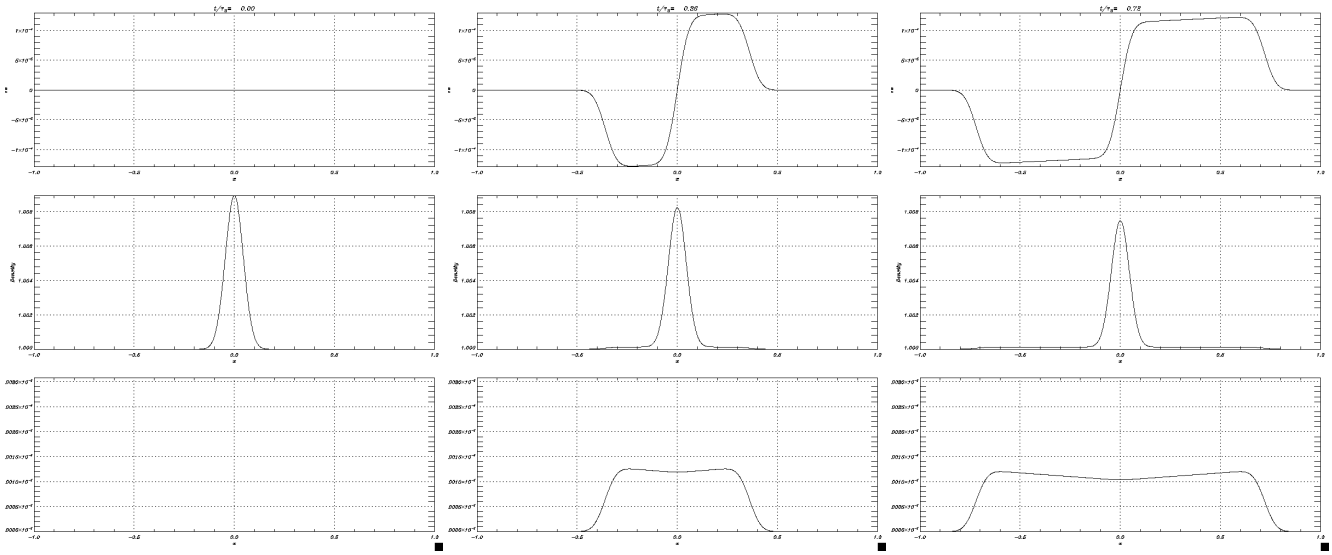

(a) t = 0 (b) t = 0.36 (c) t = 0.72

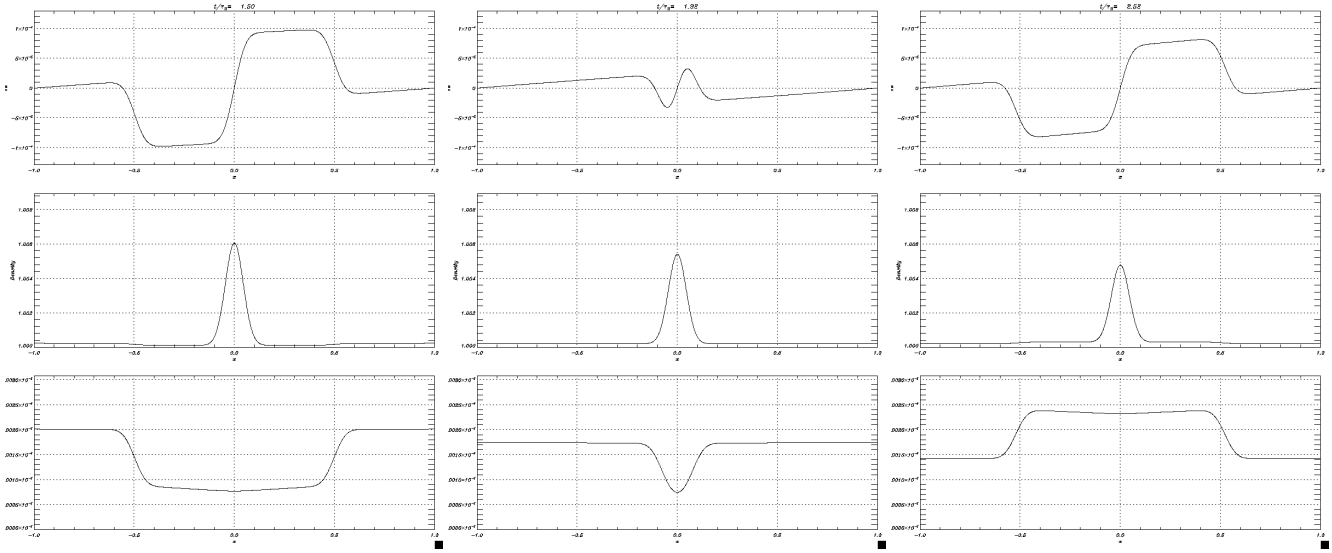

(d) t = 1.50 (e) t = 1.92 (f) t =2.52

Figure 2.12: Time evolution of a gaussian perturbation with $1 \cdot 10^4$ K plasma temperature, $\rho = 1.5 \cdot 10^{-12}$ kg m^{-3} plasma density, $A = 1 \cdot 10^{-3}$ perturbation amplitude and $L = \pi/1 \cdot 10^{-9}$ m system length. First panel is velocity in the x direction, second panel is density and third panel is pressure, all as function of space. The solid line represent the numerical result.

Chapter 3

Conclusions

In presence of high temperatures, such as the ones that can be measured at the solar corona, the effect of thermal conduction has an important contribution in terms of energy. As mentioned above, early research on the subject of this work (Balbus [6], Field [5])considers thermal conduction is negligible. Nonetheless, when we study the behaviour of the plasma in the solar atmosphere, more specifically on the solar corona, it needs to be included. Moreover, regarding the discussion about thermal instability and thermal non-equilibrium as the cause of the formation and evolution of plasma perturbation on the solar corona, we have discussed how important is thermal conduction, and it has to be included even being a stabilizing term.

In this work we have conducted several simulations along with some theoretical development. The MHD equations have been linearised and approximated according to the coronal loops features, therefore reaching a 1D approximation where the magnetic field can be neglected since plasma is moving along the field lines. When the temperature is modified with fixed density, we can obtain different situations where a perturbation has a positive growth rate or a negative growth rate. If we look again into Figure 1.8, we can see how the stability, therefore the growth rate, changes for a different temperature with a fixed density. On the simulations we can divide the perturbation evolution into a linear regime and a non-linear regime, being the linear regime the one corresponding to the analytical solution which is an exponential, thus in a logarithmic scale is displayed as a linear function. Therefore, next we took those simulations and changed the amplitude, and as we suspected, the perturbation on both cases (either negative or positive growth rate perturbations) had a longer time period evolution on the linear regime the lower the perturbation amplitude is. We encountered the same behaviour when the number of nodes was increased. Last simulations presented on this work have a Gaussian type perturbation given that is a solution that generally used to fit the observed perturbations such as coronal rain. On this case, we are no longer able to excite only one mode (since in plasma fluids acoustic modes and thermal mode are present), so a superposition of modes is expected until one of them dominates. A clear example of this phenomenon can be seen in figure 2.12, where the perturbation is dissipated while acoustic waves also appear. Nonetheless, on both cases we get the expected outcome with the given set of parameters. So, for the simulation from figure 2.11 the set of parameters corresponds to a positive growth rate (obtained from the dispersion relation), which fits with what we can observe. Same as for the simulation from figure 2.12, where the set of parameters gives a negative growth rate, which also fits with what we can observe.

Therefore, with the results presented on this thesis we are able to predict the time evolution of a perturbation given the background plasma parameters, which can be mainly represented as shown in figure 1.8. Future work will be focused on simulations of specific solar atmosphere structures, so the result of this thesis can be extended to any phenomenon on the solar atmosphere.

Bibliography

[1] Eric Priest. *Magnetohydrodynamics of the Sun*. 2014.

[2] James A. Klimchuk. The Distinction Between Thermal Nonequilibrium and Thermal Instability. *Solar Physics*, 294(12):173, December 2019.

[3] Patrick Antolin. Thermal instability and non-equilibrium in solar coronal loops: from coronal rain to long-period intensity pulsations. *Plasma Physics and Controlled Fusion*, 62(1):014016, January 2020.

[4] N. Claes and R. Keppens. Thermal stability of magnetohydrodynamic modes in homogeneous plasmas. *Astronomy and Astrophysics*, 624:A96, April 2019.

[5] G. B. Field. Thermal Instability. *The Astrophysical Journal*, 142:531, August 1965.

[6] S. A. Balbus. Local Dynamic Thermal Instability. *Astrophysical Journal, Letters*, 303:L79, April 1986.

[7] Tim Waters and Daniel Proga. Non-isobaric Thermal Instability. *The Astrophysical Journal*, 875(2):158, April 2019.

Chapter 4

Acknowledgments

Primero y ante todo, estoy muy agradecido a mi tutor, Ramon Oliver, por su inestimable orientación, su continuo apoyo y paciencia a lo largo de mi trabajo de fin de master. Su enorme conocimiento y abundante experiencia me ha animado en todo momento durante mi investigación y en mi dia a dia. Tambien quiero agradecerle su gran disponibilidad siempre que ha habido momentos dificiles a la hora de avanzar en este trabajo, y siempre que le he necesitado en un ambito personal.

Quiero dar las gracias también al Dr. Jaume Terrades por su apoyo técnico en mi tesis. También quiero agradecer a todo el grupo de física solar de la Universidad de las Islas Baleares por todas las, siempre puntuales, pausas para el café.

Por úlitmo, quiero agradecer el apoyo incondicional de mis amigos. A Aina, Albert Builes y Toni Grau porque nada más empezar el grado nos convertimos en un equipo, y desde entonces hemos hecho todo este camino juntos, lo cual ha sido un gusto. Quiero agradecerles toda la ayuda, tanto cientifica como emocional, que me han proporcionado para que este trabajo haya sido posible. A Cheik, Albert Enguita, Carlos, Gaston, Toni Segura y Chus por sacarme de casa siempre que lo necesitaba, por las risas y por los ánimos para poder continuar con este trabajo en mis peores momentos. Todos me han hecho sentir apoyado y en familia en todo momento, algo que jamás podré agradecerselo lo suficiente.

Par acabar mi agradecimiento también va a mi familia. A mi padre por su apoyo incondicional y sus valiosos consejos. A mi hermanita por siempre recibirme con un abrazo y una sonrisa en la cara cuando no estoy bien. A madre por ser siempre esa luz que ilumina mi camino más oscuro, por pensar siempre más en mi que en ella misma y por aguantar mi mal humor cuando algo va mal.